Diffusional Cross-Talk between Paired Microband Electrodes Operating within a Thin Film: Theory for Redox Couples with Unequal Diffusion Coefficients

Christian Amatore,* Catherine Sella, and Laurent Thouin

Ecole Normale Supérieure, Département de Chimie, UMR CNRS 8640 "PASTEUR", 24 rue Lhomond, 75231 Paris Cedex 05, France

Received: July 8, 2002; In Final Form: September 6, 2002

The diffusional cross-talk of reversible redox species with different diffusion coefficients was investigated theoretically at paired microband electrodes operating under generator-collector mode within a thin film coating. The influence of the diffusion coefficient ratio parameter onto the diffusion transport taking place in the restricted volume was investigated analytically by numerical simulations. A quantitative evaluation of the currents at the generator and the collector were performed in the conformal space fitted to the geometry of the device. The theory and the simulations show that several regimes of diffusion occur according to the diffusion length of the species. Analytical formulations, validated by simulations, were derived for most of these limiting behaviors. This model allows the determination of the concentrations of the redox species in the film, their individual diffusion coefficients, as well as the film thickness based on the currents monitored at the generator and collector. Its experimental validity is tested with a two-paired platinum microband assembly operating into a Nafion micrometric film in which the electrochemical reaction at the generator is the reduction of iron(III) cations.

Introduction

Electrodes coated by a polymer membrane incorporating electroactive species have been extensively studied because of the large number of applications in electrocatalytic and electrochromic systems, analysis, sensors, biosensors and other related devices.[1−3] Diffusion within these polymers is of practical importance because it controls their ability to store and transport species that are determining factors for several applications. Charge and mass transports in solid polymer matrixes including redox centers can be investigated by electrochemical methods such as chronoamperometry, chronocoulometry,[1,4] cyclic voltammetry, and steady-state and time-of-flight[5−7] methods.

The possibility of monitoring the geometrical modifications of a polymeric film in relation to its chemical environment (i.e., swelling [8,9]) and through its effects on the mass transport of incorporated redox species[10] constitutes an interesting approach in view of the conception of new kinds of sensor devices based on double-band assemblies.[11,12] The diffusion transport of reversible redox species at single and double-band microelectrodes coated with a thin film has been investigated theoretically and experimentally in a previous paper.[13] Diffusion is viewed here in a general sense, i.e., possibly involving physical diffusion−migration of free redox species within polymeric channels and diffusion−migration via electron hopping. Good agreement between theory, simulations, and experiments demonstrated that the electrochemical responses of such devices allow the diffusion transport of the redox species to be fully characterized inside the matrix as well as the physical and geometrical properties of the film. In this previous work, theory was restricted to the case where the diffusion coefficients of the reactant and the product were equal. However, the diffusion processes occurring within a polymeric matrix are expected to depend on different types of interactions between each redox state of a species and the matrix. For example, the electrostatic interactions of the reactant or product with the matrix itself depend on the charges carried by these species and whether the reaction carried out is an oxidation or a reduction process.[14] Thus, the reactant and the electrogenerated product may have very different diffusion coefficients. Note however that if the diffusion process is controlled by electron hopping only, the diffusion coefficients are formal so that their ratio is necessarily unity. A possible difference in the diffusion coefficients has no consequence on the current calculated in the single band mode (i.e., when only one of the two electrodes is electrically connected) because only the diffusion of the reactant accounts for the current-plateau monitored at the electrode. However, a difference of diffusion coefficients is expected to influence the currents when the device is operating in the generator-collector mode.

The purpose of this work was to examine the importance of this effect and thereby define the range of validity of our previous work which assumed identical diffusion coefficients. This required a new and detailed theoretical analysis which we wish to report here. We could thus develop analytical laws for most of the observable limiting behaviors and test their range of validity based on simulations.

Theory

Preliminary Considerations. The principle of the devices investigated here has been already described in our previous paper.[13] Two paired microbands are coated by a polymer thin film in which the electroactive species have been encapsulated homogeneously (Figure 1). The leakage of the redox species into the solution is considered as being negligible during the

* Corresponding author. Fax: +33-1-4432-3863. E-mail: christian.amatore@ens.fr

10.1021/jp026455n CCC: $22.00
Published on Web 10/11/2002

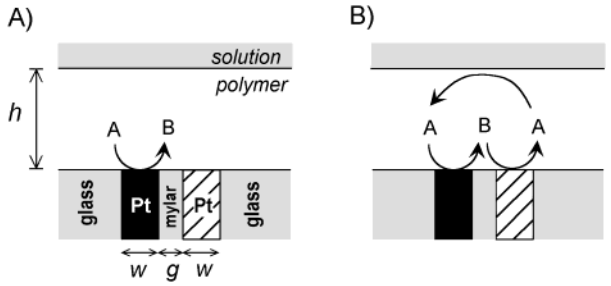

Figure 1. Schematic representations of the cross-section of the microband assemblies. (A) Single-band mode operation: only one electrode is connected (solid black). (B) Double-band mode showing the cross-talk between generator (solid black) and collector (hatched shade) electrodes: h is the thickness of the polymer film, w the width of each Pt microband, and g the width of the Mylar insulating gap. Insulating materials (glass, Mylar, bulk solution) are shown in solid gray, while the space available to diffusion is represented in white.

time duration of an experiment, in agreement with previous experimental observations.[13] The film of thickness h is supposed uniform over the whole electrode assembly and of infinite lateral dimension in comparison to the electrodes and gap widths. Under these conditions, the diffusion process occurs in a semi-infinite space under a geometrical constraint imposed by the film thickness. Microband electrodes are of width w and length l and are separated by an insulating gap of width g. The devices are characterized by their geometric dimensionless gap $\alpha = g/w$ and by their dimensionless thicknesses $\delta = 2h/w$. The two adjacent microbands are biased independently so that the electroactive species A initially present within the film is reduced (respectively oxidized) at the first electrode (generator) into a product B which thus diffuses over the gap and can be oxidized (respectively reduced) at the second electrode (collector) (Figure 1B). The species A is regenerated at the collector and diffuses back to the generator, leading to a diffusional cross-talk between the two electrodes. The magnitude of this cross-talk is time dependent and is regulated by the physical boundary condition imposed by the thickness of the film.[13,15] A theoretical evaluation of the diffusion processes occurring at these film-coated microbands was already achieved analytically and by numerical simulation upon considering identical diffusion coefficients for both the reactant A and the product B.[13] In the following, different values of the two diffusion coefficients are allowed so that a diffusion coefficient ratio r defined as D_B/D_A is introduced. The simulations were performed in a conformal space of the device to take advantage of the great simplification of the problem at hand as established previously for double band[12,13,15] and triple band electrodes[16] and interdigitated array electrodes.[17,18] These conformal spaces (see Figures 2B and 2C) have been thoroughly described in previous works of this group,[12,13,15−18] so they will not be discussed again here. In this space, the electrodes of a double band assembly face each other (Figure 2B) so that flux and isoconcentration lines are much less curved than in the real space (Figure 2A). This, however, introduces a slight difficulty in the calculations because then the film−solution interface is no longer a straight line but rather an inverted bell-shaped curve (see Figure 2B). For the best accuracy of the simulations, an appropriate grid needs thus to be defined to solve numerically the diffusion equations by finite differences.[13] The boundary conditions and algorithms are identical to those reported previously,[13] except that since the diffusion coefficients D_A and D_B differ, the simulation of each concentration profile is required rather than that of A only when $r = 1$.[13] Both diffusion fields are coupled by the conservation

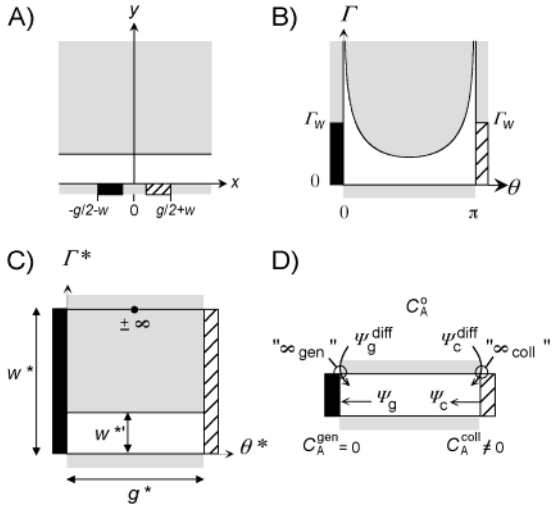

Figure 2. Geometries of the space available to diffusion for a double-band assembly in different spaces: (A) in real space (x,y); (B) in the conformal space (θ, Γ) used for the simulations of the time dependent values of Ψ_g and Ψ_c; (C) closed box conformal space used to predict analytically the steady-state current $\Psi^{\infty}_{\delta,r}$. The terms w^* and g^* are the respective widths of the electrodes and of the gap, and $w^{*\prime}$ is the equivalent width of the electrode due to the presence of the film. (D) Flux distribution in the closed box conformal space shown in (C). In A−D: generator, solid black; collector, hatched shade; insulating materials (glass, Mylar and bulk solution), solid gray; space available to diffusion, white. In B, the Γ and θ variables are defined such as $x = (g/2)\cos\theta\cosh\Gamma$ and $y = (g/2)\sin\theta\sinh\Gamma$. See ref 15 for the Γ^* and θ^* variables used in (C, D).

of fluxes as given in eq 1 at $\theta = 0$ and π for $0 \le \Gamma \le \Gamma_w$:

$$\frac{\partial c_A}{\partial \theta} + r\frac{\partial c_B}{\partial \theta} = 0 \qquad (1)$$

where θ and Γ are dimensionless space variables in the conformal space (see the conformal space in Figure 2B).

Limiting Diffusion Regimes. The dimensionless current functions $\Psi_b = i_b/[-nFlD_Ac^o_A]$, $\Psi_g = i_g/[-nFlD_Ac^o_A]$, and $\Psi_c = i_c/[nFlD_Ac^o_A]$ were defined at the single, generator, and collector microbands, respectively, and evaluated as a function of the dimensionless diffusion parameter $\underline{p}_A = (w/2)(D_At)^{-1/2}$.[13,19] The term c^o_A corresponds to the initial concentration of the reactant A homogeneously distributed within the film before the electrochemical experiment. The system is fully solved in the usual experimental situation where only one species (here A) is initially present in the film, but the analysis may be adapted to any other situation in which $c^o_B \neq 0$. Also, it is assumed that an excess of counterions is present and that these can diffuse freely within and in or out of the polymer film to compensate for the charge consumption/creation due to the electrochemical reactions at each electrode. Figure 3 shows the currents calculated for several thicknesses δ and diffusion coefficient ratios $r = D_B/D_A$ when the device operates in the single band mode (dashed lines in Figures 3A1−3A3) and in the generator-collector mode (Figures 3A1−3A3 and 3B1−3B3). These results corroborate the existence of the three limiting diffusion regimes previously identified.[13,20] These regimes depend on the duration of the experiment, i.e., on the extension of the diffusion layer as compared to the microbandwidth w and to the polymer thickness h. The currents Ψ_b, Ψ_g, and Ψ_c variations depend strongly on the thickness δ. Of particular importance is that, in contrast to Ψ_b, Ψ_g and Ψ_c depend drastically on the diffusion coefficient ratio r (Figures 3A and 3B).

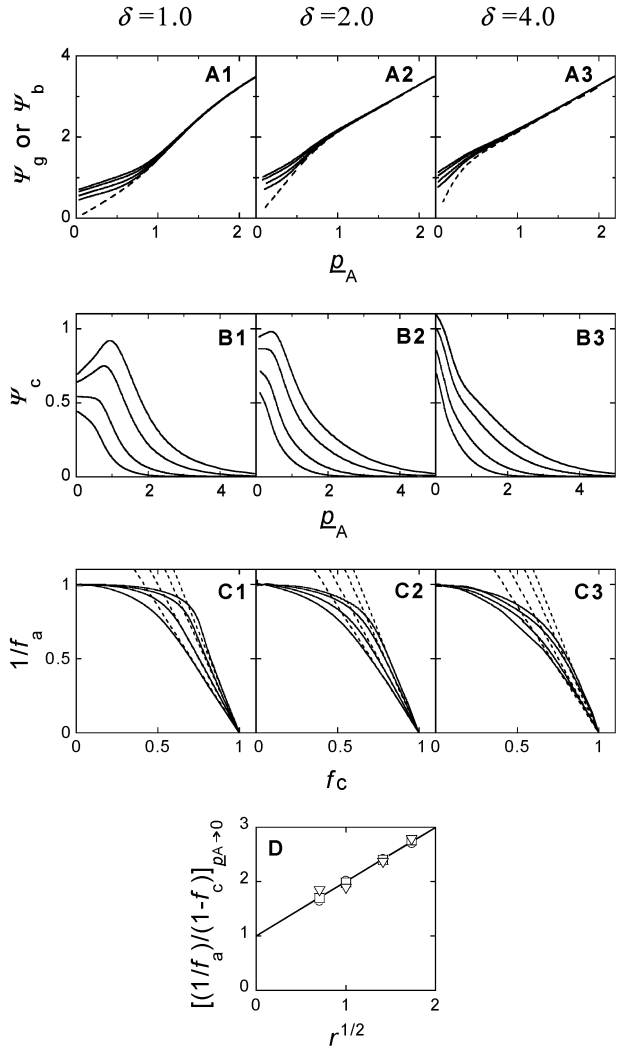

Figure 3. Dimensionless currents calculated with $\delta = 2h/w = 1.0$ (left column: A1, B1, C1), $\delta = 2.0$ (middle column: A2, B2, C2), $\delta = 4.0$ (right column: A3, B3, C3), $\alpha = g/w = 0.5$ versus $\underline{p}_A = (w/2)(D_A t)^{-1/2}$ for different diffusion coefficient ratios $r = D_B/D_A$. In each figure, solid curves correspond from bottom to top to $r = 0.5, 1, 2, 3$. (A1, A2, A3): Dimensionless current $\Psi_g = i_g/[-n\mathrm{F}lD_A c_A^o]$ at the generator (n = number of electrons exchanged). The dashed line corresponds to the dimensionless current $\Psi_b = i_b/[-n\mathrm{F}lD_A c_A^o]$ for the single band (collector off). (B1, B2, B3): Dimensionless current $\Psi_c = i_c/[n\mathrm{F}lD_A c_A^o]$ at the collector. (C1, C2, C3): Variations of the inverse of the amplification, $1/f_a = i_b/i_g = \Psi_b/\Psi_g$, as a function of the collection efficiency, $f_c = -i_c/i_g = \Psi_c/\Psi_g$, as deduced from data in (A1, A2, A3) and (B1, B2, B3); the dashed lines represent the theoretical limits achieved when $\underline{p}_A$ approaches 0 (as deduced from eq 20). (D): Variations of the slope of $1/f_a$ vs $(1 - f_c)$ at long time as determined from simulations (symbols: $\delta = 1.0$ (○), 2.0 (□), 4.0 (▽)) or predicted by eq 20 (line).

When $\underline{p}_A$ is high enough, viz., when the diffusion length is much smaller than h and w (i.e., $\underline{p}_A \gg 1$ and $\delta\ \underline{p}_A = h/(D_A t)^{1/2} \gg 1$), Ψ_b and Ψ_g are identical and are linear functions of $\underline{p}_A$ with a slope of $2\pi^{-1/2}$ while Ψ_c is negligible. This corresponds actually to semi-infinite planar diffusion at the band (or at the generator), as the diffusion layer is then a thin flat film adjacent to the generator surface whose thickness is of negligible value versus the microband width, insulating gap, and film thickness. In this case, Ψ_b and Ψ_g are given by:[15,16,19]

$$\Psi_b = \Psi_g = 1 + 2\pi^{-1/2}\underline{p}_A \qquad (2)$$

The diffusion length is so short under these circumstances that no diffusional cross-talk may occur between the bands. The generator current is independent of r and the collector current is necessarily zero (Figures 3B1−3B3).

Conversely, when $\underline{p}_A \rightarrow 0$ (i.e., $t \rightarrow \infty$) the flux lines stretch away along the polymer layer, being parallel to the insulating plane of the assembly. Diffusion becomes mostly planar over most of the development of the diffusion layer, which progresses laterally in the polymer layer as was reported previously.[13,20,21] The single band current is then proportional to $2hl$, which is twice the polymer cross-section surface area over the assembly length and Ψ_b is given by the Cottrell equation:

$$\Psi_b = i_b/[-n\mathrm{F}lD_A c_A^o] = 2\pi^{-1/2}\delta\underline{p}_A \qquad (3)$$

In this case, Ψ_g and Ψ_c tend toward a common steady-state limit $\Psi^{\infty}_{\delta,r}$, which is a function of δ and r values. The limiting current $\Psi^{\infty}_{\delta,r}$ reflects a total feedback between the generator and the collector which is reached when $\Psi_b \rightarrow 0$. Indeed, as soon as the diffusion lengths $(D_A t)^{1/2}$ and $(D_B t)^{1/2}$ become much larger than the gap width g and the film thickness h, lateral diffusional leakage becomes negligible so that a complete cross-talk takes place between the two electrodes.

Finally, a third behavior may be observed which features the transition between the two previous diffusional regimes according to δ[13] and r. However, when h and $2w+g$ are commensurate, viz., when δ and α are close to unity, this third behavior is not observable, being mixed with the transition between the two above behaviors.

Delineation of Limiting Current Laws

Effect of the Diffusion Coefficient Ratio on the Enrichment/Depletion near the Microband Surface under Steady State. To predict analytically the steady-state diffusion behavior at a double-band electrode, a second conformal space was introduced where the generator and collector electrodes face each other as in a thin layer cell (Figure 2C) and fully occupy the two opposed sides of a closed box.[15] For thin films, in this second conformal space, the region available to diffusional cross-talk is close to a thin layer cell whose electrode widths, $w^{*\prime}$, are smaller than the actual ones (vide infra, and eq 13).[13] According to the potentials held respectively at these electrodes, the concentration of species A is zero at the generator (i.e., $c_A^{gen} = 0$) and equal to a constant value c_A^{coll} at the collector. Reciprocally, the concentration of B is zero at the collector (i.e., $c_B^{coll} = 0$) and equal to c_B^{gen} at the generator (Figure 4A). Since the conservation of flux strictly applies under steady-state conditions (conservative flux), the two concentration profiles are linear in the conformal space (Figure 4A) at any location between the two electrodes. Because of eq 1, this leads to

$$D_A c_A^{coll} = D_B c_B^{gen} \qquad (4)$$

which affords

$$c_B^{gen} = \frac{D_A}{D_B} c_A^{coll} = \frac{c_A^{coll}}{r} \qquad (5)$$

In this conformal space, the location of infinity is materialized by one point located at $\theta = \pi/2$ and $\Gamma = w^*$ (Figure 2C), w^* being the microband width in this space, and where the concentrations of A and B are respectively c_A^o and 0. Thus, in a first approximation, the flux of A flowing from infinity into the closed box is proportional to $c_A^o - c_A^{coll}/2$ while the flux of B flowing out through infinity is proportional to $c_B^{gen}/2$ (Figure

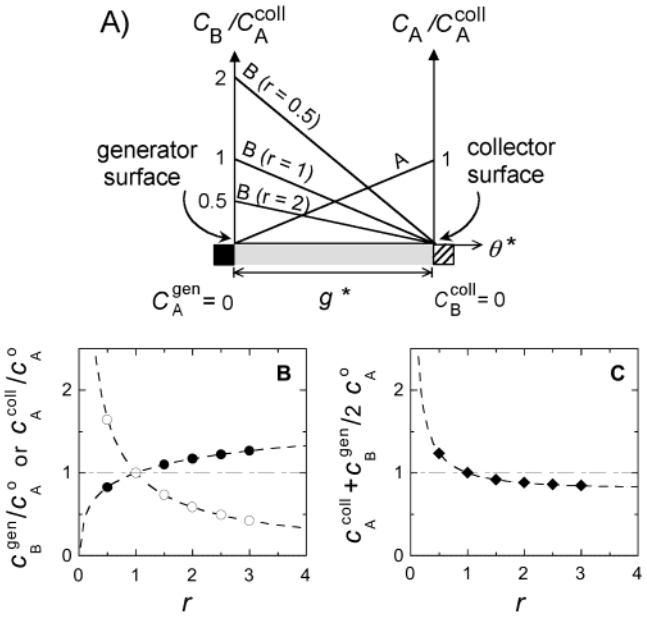

Figure 4. Concentrations c_A^{coll} and c_B^{gen} when $t \rightarrow \infty$. (A) Schematic representation of the concentration profiles of A and B, under the steady-state conditions, between the microbands assemblies operating in a generator−collector mode, for three values of r 0.5, 1 and 2, as represented as a function of θ^* in the conformal space defined in Figure 2C. (B) c_A^{coll}/c_A^o (●) and c_B^{gen}/c_A^o (○) as determined by simulations ($p_A = 0.01$) for film thicknesses varying from $\delta = 1$ to $\delta = 7$ as a function of the diffusion coefficient ratio $r = D_B/D_A$. (C) $c^{av}/c_A^o = (c_A^{coll} + c_B^{gen})/2c_A^o$ (◆) versus r, as deduced from the data in (B). The dashed curves in (B) correspond to $c_A^{coll}/c_A^o = 2\sqrt{r}/(1+\sqrt{r})$ (eq 9) and $c_B^{gen}/c_A^o = 2/\sqrt{r}\,(1+\sqrt{r})$ (eq 10) and to $c^{av}/c_A^o = (1+r)/\sqrt{r}\,(1+\sqrt{r})$ (eqs 7 and 8) in (C).

4A) (for a detailed discussion of this key feature see ref 15). When the device is coated by a thin film (viz., δ is small), we established in our previous study for $r = 1$[13] that the conformal space shown in Figure 2C was also suitable to derive analytical expressions for the limiting currents observed under the steady-state diffusion. The presence of the finite sized film could be approximated in terms of its effect by an insulating zone occupying a fraction of space (Figure 2C). This situation is then comparable to that observed for an uncoated device, except for a reduction of the width of the electrodes. Thus, diffusion proceeds as if a part of the collector was hidden to the generator. In the case of these small δ values, we have explained above that the diffusion to/from infinity (i.e., to the point $\theta = \pi/2$ and $\Gamma = w^*$ where $c_A = c_A^o$ and $c_B = 0$) occurs through the two top corner angles of the reduced closed box (see Figure 2D) and is planar due to the limitation by the film at large lateral distances from the assembly (see Figures 3A1−3A3). Thus, diffusional fluxes are Cottrellian, i.e., proportional to the square root of diffusion coefficients. Therefore, the conservation of lateral diffusional fluxes imposes

$$\left[c_A^o - \frac{c_A^{coll}}{2}\right]\sqrt{D_A} = \frac{c_B^{gen}}{2}\sqrt{D_B} \tag{6}$$

Combining eq 6 with eq 4 leads to the evaluation of c^{av}, the average A/B concentration in the vicinity of the paired bands:

$$c^{av} = \frac{1}{2}(c_A^{coll} + c_B^{gen}) = c_A^o f_{pl}(r) \tag{7}$$

with

$$f_{pl}(r) = \left[\frac{\sqrt{r}\left(1+\frac{1}{r}\right)}{1+\sqrt{r}}\right] \tag{8}$$

Equation 7 shows that, depending on r, there is an accumulation ($r < 1$) or a depletion ($r > 1$) of matter in the vicinity of the electrodes. The term $f_{pl}(r) \neq 1$ accounts for the unbalance between the initial concentration c_A^o and the average concentration c^{av} when D_A and D_B differ. It is noteworthy that $f_{pl}(r)$ is only equal to unity when $r = 1$. In this particular case, the flux conservation law, which applies at any location between the two electrodes, features exactly the mass conservation law. When $r \neq 1$, the concentrations of A and B at the electrode surface can be estimated by combining eq 5 with eq 7. Thus

$$c_A^{coll} = 2c_A^o\sqrt{r}/(1+\sqrt{r}) \tag{9}$$

$$c_B^{gen} = 2c_A^o/\sqrt{r}(1+\sqrt{r}) \tag{10}$$

which are represented as a function of r in Figure 4B, as well as c^{av}/c_A^o (Figure 4C). The values of c_A^{coll} and c_B^{gen} were also obtained through simulations imposing any assumptions. The simulated results c_A^{coll}/c_A^o and c_B^{gen}/c_A^o obtained for small p_A values are also reported in Figure 4B as a function of r for different thicknesses δ. The simulated concentrations vary as predicted analytically above (eqs 9 and 10), and the film thickness was shown to play no role on the concentrations, provided that δ is not excessively large ($\delta < 10$) (note that it will have nevertheless an effect on the current values which depend then on $w^{*\prime}$ (see below)). The values of c_A^{coll} and c_B^{gen} differ from c_A^o except when $r = 1$. The influence of r onto c_A^{coll}/c_A^o is less significant than onto c_B^{gen}/c_A^o and is significant only for very small r values. The influence of r on c_B^{gen}/c_A^o is more significant. Indeed, a large enrichment in species B is noticed through the values of $c_B^{gen}/c_A^o > 1$ when $r < 1$ (Figure 4B) while a large depletion phenomena is observed when $r > 1$ (i.e., $c_B^{gen}/c_A^o < 1$). Interestingly, as predicted by eqs 7 and 8, the overall matter depletion, (viz., $c^{av}/c_A^o < 1$) is not severe when $r > 1$, but the enrichment is extremely significant when $r < 1$ (see Figure 4C).

Effect of the Diffusion Coefficient Ratio on the Limiting Current $\Psi_{\delta,r}^{\infty}$. Figure 3 establishes that at long times the generator and collector currents tend toward the same constant limit $\Psi_{\delta,r}^{\infty}$, which is a function of δ and r. We wish to establish here some properties of this limit.

On the basis of the conformal space analysis used for the evaluation of steady-state diffusion concentrations (Figure 2C and 4A), the limiting current $\Psi_{\delta,r}^{\infty}$ can be estimated for any thickness δ and any diffusion coefficient ratio r by the following equation:

$$\Psi_{\delta,r}^{\infty} = \frac{c_A^{coll}}{c_A^o}\Psi_{\delta,1}^{\infty} \tag{11}$$

where $\Psi_{\delta,1}^{\infty}$ is the limiting current achieved for $r = 1$.[13] In this relation, the concentration ratio c_A^{coll}/c_A^o accounts for the influence of r through the enrichment/depletion of species A in the close vicinity of the electrodes (Figure 4). When the film thickness is small, eq 9 applies and its combination with eq 11

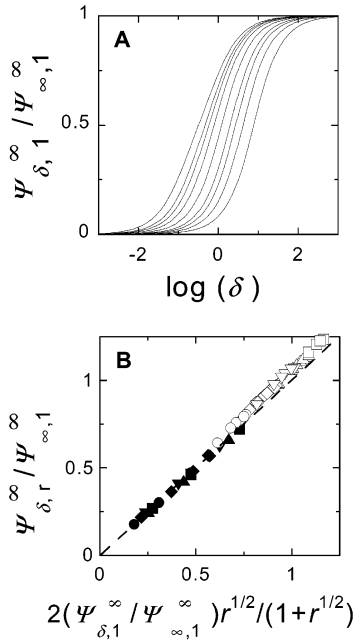

Figure 5. (A) Variations of $\Psi^{\infty}_{\delta,1}/\Psi^{\infty}_{\infty,1}$ as predicted by eq 13 as a function of log(δ) for different values of α; from left to right $\alpha = 0.1$, 0.2, 0.3, 0.5, 1.0, 2.0, 3.0, 5.0, 10. (B) Values of the ratio $\Psi^{\infty}_{\delta,r}/\Psi^{\infty}_{\infty,1}$ calculated from the values of $\Psi^{\infty}_{\delta,r}$ extrapolated at infinite time (see text and Figure 6A) based on simulations for $\alpha = 0.5$ and different values of δ (ranging from 0.25 to 7; filled symbols for $\delta \leq 1$ and open symbols for $\delta > 1$) and $r = D_B/D_A$ ($r = 0.5$ (○,●), 1.0 (◇,◆), 1.5 (▽,▼), 2.0 (△, ▲), 3.0 (□, ■)) as a function of $2(\Psi^{\infty}_{\delta,1}/\Psi^{\infty}_{\infty,1})\sqrt{r}/(1 + \sqrt{r})$ (see eq 12). Nota Bene: the value of $\Psi^{\infty}_{\infty,1}$ is equal to 0.95 when $\alpha = 0.5$.[15]

affords

$$\frac{\Psi^{\infty}_{\delta,r}}{\Psi^{\infty}_{\infty,1}} = 2\frac{\sqrt{r}}{1+\sqrt{r}}\frac{\Psi^{\infty}_{\delta,1}}{\Psi^{\infty}_{\infty,1}} \qquad (12)$$

where $\Psi^{\infty}_{\infty,1}$ is the limiting current obtained for an infinite film thickness (viz., $\delta \rightarrow 8$) and for a diffusion coefficient ratio r equal to 1. The current ratio $\Psi^{\infty}_{\delta,1}/\Psi^{\infty}_{\infty,1}$ is by definition independent of r and was shown previously to be given by the following equation:[13]

$$\frac{\Psi^{\infty}_{\delta,1}}{\Psi^{\infty}_{\infty,1}} \approx \frac{\int_0^{1.41\delta}[(z^2+\alpha^2)(z^2+(2+\alpha)^2)]^{-1/2}\,dz}{\int_{\alpha}^{2+\alpha}[(z^2-\alpha^2)((2+\alpha)^2-z^2)]^{-1/2}\,dz} \qquad (13)$$

The variations of $\Psi^{\infty}_{\delta,1}/\Psi^{\infty}_{\infty,1}$ as a function of logδ are reported in Figure 5A for different values of α. This allows to predict (eqs 12 and 13) the influence of r onto the limiting current $\Psi^{\infty}_{\delta,r}$. Indeed, the term $2\sqrt{r}/(1+\sqrt{r})$ shows that $\Psi^{\infty}_{\delta,r} > \Psi^{\infty}_{\delta,1}$ for $r > 1$, which reflects the moderate enrichment of the reactant A at the collector surface, and conversely it shows that $\Psi^{\infty}_{\delta,r} < \Psi^{\infty}_{\delta,1}$ for $r < 1$, which stresses the important depletion of A under these conditions (Figure 4B).

The limiting current $\Psi^{\infty}_{\delta,r}$ was also evaluated by extrapolation at zero $\underline{p}_A$ values of the simulated currents Ψ_g and Ψ_c obtained at a series of small $\underline{p}_A$ values as illustrated in Figure 6A for $r = 2$ and $\delta = 4$ ($\alpha = 0.5$). The value of $\Psi^{\infty}_{\infty,1}$ is equal to 0.95 when $\alpha = 0.5$.[15] The corresponding simulated values of $\Psi^{\infty}_{\delta,r}/\Psi^{\infty}_{\infty,1}$ are reported in Figure 5B. The processing of all the simulated currents for different values of δ and r ($0.25 \leq \delta \leq 7$ and $0.5 \leq r \leq 3$) shows that $\Psi^{\infty}_{\delta,r}/\Psi^{\infty}_{\infty,1}$ follows eq 12 within a remarkable accuracy. Nevertheless, one observes a slight deviation from this relationship for values of $\Psi^{\infty}_{\delta,r}/\Psi^{\infty}_{\infty,1}$ higher than 0.7 (which correspond approximately to δ higher than 1). This is observed whatever the value of r. Indeed, one must note that because eq 12 is a consequence of eq 6, it is strictly valid only when planar diffusion is fully achieved without any component from cylindrical diffusion.[15] Consequently, eq 12 is strictly valid only when the thickness of the film is small enough. For $\delta > 1$, a mixed diffusion regime starts to take place involving a slight contamination by cylindrical diffusion. This increases with δ, so that the results are expected to depend on the exact geometry of the device (compare Figures 3A1−3A3). However, it is striking that the resulting deviations from the pure planar diffusion case remain extremely modest (Figure 5B).

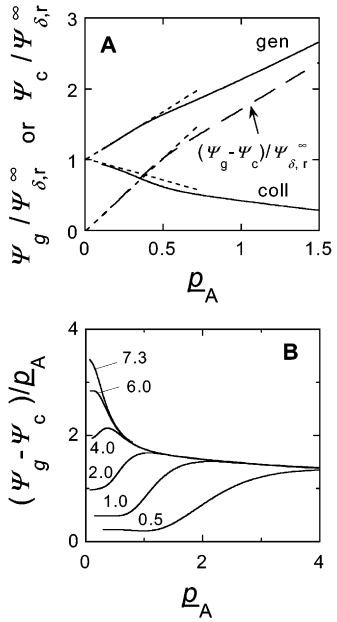

Figure 6. (A) Simulated variations of $\Psi_g/\Psi^{\infty}_{\delta,r}$, $\Psi_c/\Psi^{\infty}_{\delta,r}$, and of the difference $(\Psi_g - \Psi_c)/\Psi^{\infty}_{\delta,r}$ versus $\underline{p}_A$ for $\delta = 4.0$, $\alpha = 0.5$ and $r = 2.0$ (note that here $\Psi^{\infty}_{4,2} = 1.02$); the variations of $(\Psi_g - \Psi^{\infty}_{\delta,r})/\Psi^{\infty}_{\delta,r}\,\underline{p}_A$, $(\Psi_c - \Psi^{\infty}_{\delta,r})/\Psi^{\infty}_{\delta,r}\,\underline{p}_A$, and $(\Psi_g - \Psi_c)/\Psi^{\infty}_{\delta,r}\underline{p}_A$ when $\underline{p}_A \leq 0.2$ are reported in dashed lines. (B) $(\Psi_g - \Psi_c)/\underline{p}_A$ plots versus $\underline{p}_A$ for $r = 2$ and various δ (the values of δ are reported on the figure).

Effect of the Diffusion Coefficient Ratio on Ψ_g and Ψ_c at Noninfinite Times. Upon reaching infinite times (i.e., $\underline{p}_A \ll 1$), the system tends toward steady state as is apparent in Figures 3 and 6 for example. When $\underline{p}_A = 0$ the collector current exactly balances the generator current (Figure 6A). Then $\Psi_g = \Psi_c = \Psi^{\infty}_{\delta,r}$ while c_A^{coll} and c_B^{gen} have their values estimated above through eqs 9 and 10. This occurs because the lateral fluxes have become negligible. However when time is large but not infinite, the diffusional lateral fluxes cannot be neglected. This creates a slight unbalance between Ψ_g and Ψ_c (see, e.g., Figures 3 and 6A). The conservation of fluxes active in the closed box conformal space schematized in Figure 2D gives readily for species A:

$$\Psi_g = \Psi_c + \Psi_g^{diff} + \Psi_c^{diff} \qquad (14)$$

where Ψ_g^{diff} and Ψ_c^{diff} are the currents flowing to infinity along the inactive portions of the electrode surfaces, respectively, through the points labeled "∞_{gen}" and "∞_{coll}" in Figure 2D. For a detailed discussion of this key feature see ref 13.

In the following we restrict the discussion to the case of major experimental importance to us, i.e., when the polymer film is

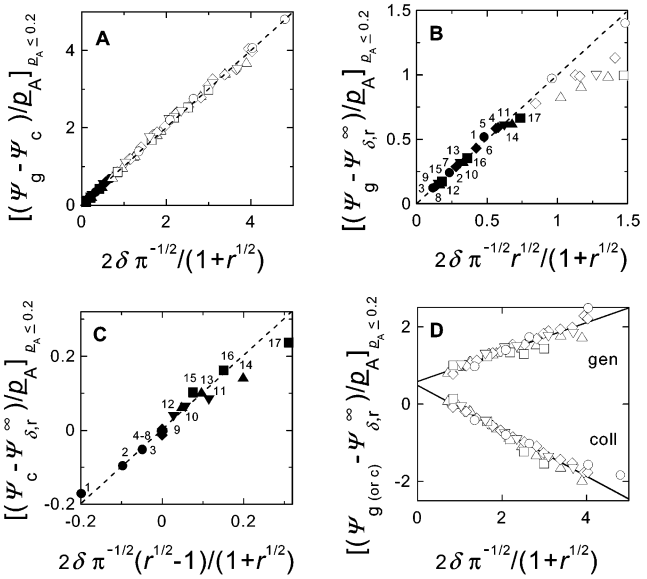

Figure 7. (A) Values of $[(\Psi_g - \Psi_c)/\underline{p}_A]_{\underline{p}_A\le 0.2}$ as determined from simulated Ψ_g and Ψ_c current functions at long times ($\underline{p}_A \le 0.2$; see Figure 6), as a function of $2\pi^{-1/2}\delta/(1+\sqrt{r})$ (eq 15) for different δ ranging from 0.25 to 7 (filled symbols for $\delta \le 1$ and empty symbols for $\delta > 1$) and diffusion coefficient ratios $r = D_B/D_A$ ($r = 0.5$ (○,●), 1.0 (◇,◆), 1.5 (▽,▼), 2.0 (△, ▲), 3.0 (□, ■)). (B) Values of $[(\Psi_g - \Psi^{\infty}_{\delta,r})/\underline{p}_A]_{\underline{p}_A\le 0.2}$ when $2\pi^{-1/2}\delta/(1+\sqrt{r}) < 1$ as a function of $2\pi^{-1/2}\delta\sqrt{r}/(1+\sqrt{r})$ (eq 17). (C) Values of $[(\Psi_c - \Psi^{\infty}_{\delta,r})/\underline{p}_A]_{\underline{p}_A\le 0.2}$ when $\delta \le 1$ as a function of $2\pi^{-1/2}\delta$ $(\sqrt{r}-1)/(1+\sqrt{r})$ (eq 18). The points labeled with the same number in (B) an (C) are calculated for the generator and collector currents obtained in the same simulation (same r and same δ) and at the same $\underline{p}_A$ value. (D) Values of $[(\Psi_g - \Psi^{\infty}_{\delta,r})/\underline{p}_A]_{\underline{p}_A\le 0.2}$ and $[(\Psi_c - \Psi^{\infty}_{\delta,r})/\underline{p}_A]_{\underline{p}_A\le 0.2}$ when $\delta > 1$ (i.e., $2\pi^{-1/2}\delta/(1+\sqrt{r}) > 0.8$) as a function of $2\pi^{-1/2}\delta/(1+\sqrt{r})$. Linear regression equations (dashed lines): generator, $y = 0.53 + 0.40x$ (corr. coeff. $R = 0.951$); collector, $y = 0.53 - 0.60x$ (corr. coeff. $R = 0.980$).

actually a thin strip, viz., when δ is not large compared to unity. Under such conditions, we have shown above that Ψ_g^{diff} and Ψ_c^{diff} (Figure 2D and eq 14) are Cottrellian-like currents: Ψ_g^{diff} and Ψ_c^{diff} are proportional to $\underline{p}_A$ and correspond to a fictitious electrode surface area equal to that of the cross-section of the film (e.g., $1/2\delta wl$ where the factor 1/2 stems from the fact that by definition the lateral diffusional fluxes Ψ_g^{diff} and Ψ_c^{diff} proceed only from one side of the assembly). Because the generator potential imposes $c_A^{gen} = 0$ at the point labeled "∞_{gen}" in Figure 2D and $c_A^{gen} = c_A^o$ at infinity, then Ψ_g^{diff} is proportional to c_A^o. Conversely, because the collector potential imposes $c_A^{coll} \neq 0$ at the point labeled "∞_{coll}", Ψ_c^{diff} is proportional to $c_A^o - c_A^{coll}$, where c_A^{coll} is given in eq 9. Thus eq 14 is readily rewritten as

$$\Psi_g = \Psi_c + 2\pi^{-1/2}\delta\frac{1}{1+\sqrt{r}}\underline{p}_A \qquad (15)$$

Simulations were performed for several values of δ ($0.25 \le \delta \le 7$) and r ($0.5 \le r \le 3$) as a function of $\underline{p}_A$, and their results are presented in Figure 7A under the form of the limit of the difference between Ψ_g and Ψ_c divided by $\underline{p}_A$ when $\underline{p}_A \ll 1$ (viz., $\underline{p}_A \le 0.2$). It is clear from Figure 7A that the relationship in eq 15 is strictly obeyed as soon as $\underline{p}_A$ is small and not only for infinitely small values of this parameter.

At very long times (i.e., $\underline{p}_A \ll 1$), we demonstrated previously[13] that for $r = 1$ the current Ψ_g can be also expressed as a sum of two contributions, assuming that the diffusional process between the two electrodes is almost under steady state while the diffusion from the generator side (opposed to the collector) still follows a Cottrellian behavior:

$$\Psi_g = \Psi^{\infty}_{\delta,1} + \Psi_g^{diff}\,(r = 1) \qquad (16)$$

On the basis of the analytical model described in Figure 4A, it is seen that the role of r onto the current Ψ_g introduces only a multiplying factor equal to c_A^{coll}/c_A^o in the right-hand side of eq 16. Using eqs 9 and 11, eq 16 is then rewritten as

$$\Psi_g = \Psi^{\infty}_{\delta,r} + 2\pi^{-1/2}\delta\frac{\sqrt{r}}{1+\sqrt{r}}\underline{p}_A \qquad (17)$$

Ψ_c is then readily obtained by combination of eqs 17 and 15, so that

$$\Psi_c = \Psi^{\infty}_{\delta,r} - 2\pi^{-1/2}\delta\frac{1-\sqrt{r}}{1+\sqrt{r}}\underline{p}_A \qquad (18)$$

This establishes that both Ψ_g and Ψ_c reach their common limit $\Psi^{\infty}_{\delta,r}$ by varying linearly with $\underline{p}_A$ as soon as the local steady-state regime is achieved (i.e., for $\underline{p}_A \to 0$; compare Figure 6A). However, the slopes of Ψ_g and Ψ_c differ, which evidences the strong dissymmetry of the diffusional feed on each side of the system. Interestingly, when $r \approx 1$, the slope of Ψ_c is considerably smaller than that of Ψ_g, which shows that the collector current reaches steady-state sooner than the generator current as noted previously.[13,15]

To test the range of validity of eqs 17 and 18, we relied on simulations without introducing any of the above assumptions. The results of these simulations are presented in Figures 7B and 7C under the form of the limit of the differences between Ψ_g or Ψ_c and $\Psi^{\infty}_{\delta,r}$ divided by $\underline{p}_A$ when $\underline{p}_A \le 0.2$. These two plots evidence the validity of the two analytical limits in eqs 17 and 18. However, these limits are observed only over a range of values of $\delta/(1+\sqrt{r})$ smaller than eq 15. This is illustrated in Figure 7A where the range of validity of eqs 17 and 18 is indicated by the filled symbols. In fact, the simulated data in Figure 7D (which correspond to the data shown in open symbols in Figure 7A) establish that when $\delta/(1+\sqrt{r})$ is larger than ca. 0.8, eqs 17 and 18 are no longer obeyed but that $\Psi_g - \Psi^{\infty}_{\delta,r}$ and $\Psi_c - \Psi^{\infty}_{\delta,r}$ vary linearly with $\delta\,\underline{p}_A/(1+\sqrt{r})$. Thus, the set of Figures 7B−D demonstrates that two regimes actually occur on each side of a threshold value (~0.8) of $\delta/(1+\sqrt{r})$. For lower values of this parameter, Ψ_g and Ψ_c follow, respectively, eqs 17 and 18 with the expected slopes as shown in Figures 7B and 7C, showing that these equations are valid only when planar diffusion occurs and consequently are valid only when the thickness of the film is small enough ($\delta \le 1$). Conversely, when $\delta > 1$ (i.e., $2\pi^{-1/2}\delta/(1+\sqrt{r}) > 0.8$, empty symbols in Figure 7), the situation becomes more complicated presumably because it corresponds to a mixed diffusional regime imposed by cylindrical/planar diffusion at the edges of each electrode, which affects the diffusion cross-talk between the microbands. Interestingly, this effect is symmetrical for Ψ_g and Ψ_c, so that it cancels off when their difference is considered. Therefore, eq 15 remains valid over a large range of δ and r values (Figure 7A).

Effect of the Diffusion Coefficient Ratio onto Collection and Amplification Factors. Under quasi steady-state condi-

tions, combining eqs 3 and 15 leads to the following expression:

$$1 = \frac{\Psi_c}{\Psi_g} + \frac{1}{1+\sqrt{r}}\frac{\Psi_b}{\Psi_g} \tag{19}$$

where the quantities Ψ_c/Ψ_g and Ψ_b/Ψ_g are usually defined as the collection efficiency f_c and the inverse of the amplification factor $1/f_a$, respectively.[13,15,19] Eq 19 may then be rewritten as

$$\frac{1}{f_a} = [1+\sqrt{r}][1-f_c] \tag{20}$$

which shows that $1/f_a$ is proportional to $(1 - f_c)$ under steady-state conditions as it has been observed for other generator−collector microband assemblies.[13,15] In fact, the variation of $1/f_a$ versus f_c may be used to characterize the electrochemical behavior of the device at any time [13,15] and was found previously to be also dependent on δ ($r = 1$).[13] Figures 3C1−3C3 show that this previous result is conserved when $r \neq 1$, yet one observes that the slope of $1/f_a$ vs $(1 - f_c)$ at long times also depends on r. Figure 3D shows in fact that the prediction in eq 20 is actually remarkably followed by the simulated results (i.e., obtained without any assumption).

Thus, in each case, two asymptotic behaviors are observed. On one hand, when time is sufficiently short, the diffusion layer at the generator does not extend across the gap, so that $\Psi_g = \Psi_b$ and thus $1/f_a = 1$ and $f_c = 0$. On the other hand, at long time, when the steady-state regime is approached, $1/f_a$ tends to 0 and f_c tends to 1. Then, $1/f_a$ varies linearly with $(1 - f_c)$ with a slope that does not depend on δ [13] and is equal to $(1 + \sqrt{r})$, as predicted by eq 20. The thinner the film is or the higher r is, the sooner this steady-state limit is reached, which is in full agreement with the prediction in eqs 17 and 18.

Conclusion

We examined analytically and by simulation the influence of the diffusion coefficient ratio r between the reactant and the product onto the diffusional transport at double-band microelectrodes within a coated film. These results show that at any given film thickness the value of r controls significantly the currents monitored at the device when it is operated in the generator−collector mode. The theoretical analytical limits of the currents at steady state were investigated and established as well as the analytical expressions of the concentrations of species near the microbands surface. These results show a good agreement with the simulated currents near steady state. Thus, this study affords the opportunity to examine quantitatively the experimental responses of such devices in particular in view of extracting the electrochemical and geometrical parameters which characterize the diffusion within the film. Work is under progress in our laboratory in this direction and will be reported soon.

Acknowledgment. This work has been supported in part by the CNRS (UMR 8640), the French Ministry of Research (Action Spécifique DGRT N° 97.1502), and by the Ecole Normale Supérieure. F. Grün and Dr. J-S. Warkocz are gratefully acknowledged for their help in programming in C language. UMR 8640 is associated to CNRS, ENS, and to University Pierre et Marie Curie.

References and Notes

(1) Murray, R. W. *Molecular design of electrode surfaces*; Wiley & sons, Inc.: New York, 1992; Vol. XXII.
(2) Chidsey, C. E.; Feldman, B. J.; Lundgren, C.; Murray, R. W. *Anal. Chem.* **1986**, *58*, 601.
(3) Inzelt, G. In *Electroanalytical Chemistry*; Bard, A. J., Ed.; Marcel Dekker: New York, 1994; Vol. 18; p 89.
(4) Anson, F. C.; Blauch, D. N.; Savéant, J.-M.; Shu, C.-F. *J. Am. Chem. Soc.* **1991**, *113*, 1922.
(5) Feldman, B. J.; Feldberg, S. W.; Murray, R. W. *J. Phys. Chem.* **1987**, *91*, 6558.
(6) Licht, S.; Cammarata, V.; Wrighton, M. S. *J. Phys. Chem.* **1990**, *94*, 6133.
(7) Wittek, M.; Möller, G.; Johnson, M. J.; Majda, M. *Anal. Chem.* **2001**, *73*, 870.
(8) Albert, K. J.; Lewis, N. S.; Schauer, C. L.; Sotzing, G. A.; Stitzel, S. E.; Vaid, T. P.; Walt, D. R. *Chem. Rev.* **2000**, *100*, 2595.
(9) White, J.; Kauer, J. S.; Dickinson, T. A.; Walt, D. R. *Anal. Chem.* **1996**, *68*, 2191.
(10) Geng, G.; Reed, R. A.; Kim, M.-H.; Wooster, T. T.; Oliver, B. N.; Egekeze, J.; Kennedy, R. T.; Jorgenson, J. W.; Parcher, J. F.; Murray, R. W. *J. Am. Chem. Soc.* **1989**, *111*, 1614.
(11) Amatore, C.; Brown, A. R.; Thouin, L.; Warkocz, J. S. *C. R. Acad. Sci. Paris* **1998**, *t. 1*, 509.
(12) Amatore, C.; Thouin, L.; Warkocz, J. S. *Chem. Eur. J.* **1999**, *5*, 456.
(13) Arkoub, I.-A.; Amatore, C.; Sella, C.; Thouin, L.; Warkocz, J.-S. *J. Phys. Chem. B* **2001**, *105*, 8694.
(14) Zhang, J.; Zhao, F.; Abe, T.; Kaneko, M. *Electrochim. Acta* **1999**, *45*, 399.
(15) Fosset, B.; Amatore, C.; Bartelt, J. E.; Michael, A. C.; Wightman, R. W. *Anal. Chem.* **1991**, *63*, 306.
(16) Fosset, B.; Amatore, C.; Bartelt, J.; Wightman, R. M. *Anal. Chem.* **1991**, *63*, 1403.
(17) Aoki, K.; Morita, M.; Niwa, O.; Tabei, H. *J. Electroanal. Chem.* **1988**, *256*, 269.
(18) Postlethwaite, T. A.; Hutchison, J. E.; Murray, R. W.; Fosset, B.; Amatore, C. *Anal. Chem.* **1996**, *68*, 2951.
(19) Amatore, C. Electrochemistry at ultramicroelectrodes. In *Physical Electrochemistry*; Rubinstein, I., Ed.; Marcel Dekker: New York, 1995; p 131.
(20) Ferrigno, R.; Brevet, P. F.; Girault, H. H. *J. Electroanal. Chem.* **1997**, *430*, 235.
(21) Compton, R. G.; Fisher, A. C.; Wellington, R. G.; Dobson, P. J.; Leigh, P. A. *J. Phys. Chem.* **1993**, *97*, 10410.